Jestr

Journal of Engineering Science and Technology Review 15 (SI) (2022) 49 - 62
Special Issue in honor of Prof. T. Tanaka

JOURNAL OF
Engineering Science and Technology Review

Review Article

www.jestr.org

A Brief Review of Thermal Mechanism of Failure in Power Cable Insulation

CC Reddy*

Senior Member, IEEE, Purnabhishek Muppala, Sathyamoorthy Dhayalan

Received 1 February 2022; Accepted 10 March 2022

Abstract

It is being increasingly recognized that the mechanism of failure in power cables is of thermal in nature. Several authors since Whitehead and O'Dwyer had worked on this topic, however considering recent advances, this paper presents a brief review of mechanisms of breakdown in power cables, both under steady state and transient conditions while mainly focusing on the thermal mechanism. This helps both in formation of concrete theory for the phenomenon that is statistical in nature and also predict the breakdown in insulation with just its material properties.

Keywords: Thermal Breakdown, DC Cables, electric field distribution, temperature distribution, Maximum Thermal Voltage (MTV)

1. Introduction

THE failure of HVDC cable insulation (especially polymeric insulation) can be traced down to electro-thermal instability. The electric field distribution inside the insulation matrix is dependent on its conductivity, which in turn is a strong non-linear function of electric field and temperature at that point. The temperature rise in the insulation is primarily due to the Ohmic losses in the conductor and the leakage current in the insulation, the latter which is compoundingly dependent on field and temperature. Thermal instability occurs primarily due to this non-linearity.

Electrical conduction and breakdown in dielectrics has been a subject of discussion for a long time. The earliest works in this area were of Semenoff, Fröhlich, Von Hippel et al [1-4] who had investigated conduction in dielectrics under low and high fields by considering the effects of electrodes, their material and surface characteristics. Based on these studies, the processes leading to purely electrical breakdown were proposed by Whitehead, Austen, Pelzer, Inge and Walther [5-8]. These works focused on dielectrics with a predefined molecular structure.

Later on, Whitehead and O'Dwyer [9, 10] realized the importance of mechanisms of conduction and its connection to thermal effects in breakdown. They have proposed the models for computing approximate breakdown fields in commercial polymers for planar and cylindrical geometries under fixed and ambient boundary temperatures.

Since then, several experimental observations indicated the exponential dependence of conductivity on electric field and temperature, yet obtaining a closed form function for conductivity that is applicable to all dielectrics, at all fields and temperatures was found to be difficult and often untenable. Several models were proposed by different authors [11-15], however they were limited to certain class of dielectrics, and field and temperature ranges.

For a long time thereafter, the research was only confined to material experiments and it wasn't until early 1970's with the advent of high voltage power cable transmission that the interest on this topic was revived. Experiments had shown a reduction in DC breakdown strength of polyethylene and oil impregnated cables with increase in ambient and conductor temperature difference [16].

The works of Whitehead, O'Dwyer [9, 10] and Fallou [17] have neglected the electric stress dependence of conductivity, perhaps for the sake of simplicity. The temperature dependence they used were also different from Boltzmann dependence. Later on, Eoll [18, 19] and Jeroense [20] realized the significance of electric field dependence and have proposed analytical expressions for electric stress with reasonable accuracy, with certain approximations in the conductivity equation. However, a proper closed form mathematical model for electric stress distribution, temperature and breakdown fields that is valid for all conditions was first proposed by the author [21]. A connection between breakdown and thermal instability was established, and the mechanism of thermal failure was codified.

The thermal instability in dielectrics involves two components, intrinsic (internal) and interactive instability. The interactive instability is dependent on external thermal resistance, whereas intrinsic instability is solely due to the nonlinear conductivity of the material.

The concept of intrinsic instability (specific to DC cables) was first postulated by Eoll [18, 19]. While Fallou [17] and Jeroense [20] have also worked on certain aspects of thermal breakdown, the concept of intrinsic thermal breakdown was not recognized by them, either due to inadequate incorporation of leakage current losses or due to electric field dependence on conductivity being ignored. It was the author who dealt with this elaborately in his subsequent work [22] and developed the concept of intrinsic thermal maximum voltage (IMTV). Based on this, the maximum power handling capacity of a HVDC cable was formulated for the first time [23].

From these results, several models, both mathematical and numerical, for electric field, space charge, temperature distribution and breakdown in sundry dielectrics and

*E-mail address: reddy@iitrpr.ac.in

doi:10.25103/jestr.147.08

dielectric configurations [24-27] including composite dielectrics such as cable joints [28] came into picture.

Existing literature is scarcer when it comes to the transient thermal behavior of HVDC cables. While some finite element models (FEM) are reported [29-32] they are however wrought with limitations such as neglecting leakage current losses in insulation or not considering nonlinear conductivity or not considering electric field dependence etc., that are shown to cause convergence difficulties in their models near breakdown. The same is the case with circuit models [33-35], where thermal capacitances are not considered, or leakage current losses were lumped or neglected altogether. It wasn't until the author [36], a circuit model that can simulate complete thermal and electrical behavior of the cable under transient conditions, including thermal runaway, was proposed.

This review paper will briefly introduce conductivity models before beginning from Whitehead and O'Dwyer's thermal breakdown models in plane parallel geometry (steady state) and then expounds on thermal breakdown in DC cables (steady state). The circuit model for dc cable which simulates complete transient behavior of DC cable is also explored.

2. Models for Electrical Conductivity

As mentioned in the previous section, a theoretical model for the conductivity that is applicable to all kinds of solid dielectrics for all fields and temperature ranges is not yet available. There are only semi-empirical models that are applicable for limited dielectrics and field and temperature ranges.

The first model was proposed by Austen and Whitehead [5, 6, 9] which is of the following form.

$$\sigma = Ae^{\frac{-b}{T}}\left(\frac{e^{aE/2kT}-e^{-aE/2kT}}{2(1-e^{-aE/2kT})}\right) \quad (1)$$

This above equation can be compacted to Blythe's form [12]

$$\sigma = Ae^{\frac{-b}{T}}\left(\frac{sinh\left(\frac{aE}{2kT}\right)}{(1-e^{-aE/2kT})}\right) \quad (2)$$

The disadvantage of this model is that, the stress related enhancement in the conductivity is only marginal.

Later, two different models were proposed for polymeric materials, one by Boggs [13, 14] and another by Klein [15]. The Boggs' equation is shown below.

$$\sigma = A'e^{\frac{-b}{T}}\left(\frac{sinh(B|E|)}{|E|}\right) \quad (3)$$

Klein's equation is shown below.

$$\sigma = Ae^{\frac{-b}{T}}e^{a|E|} \quad (4)$$

Boggs' equation is slightly more accurate; however, it often runs into convergence problems when used in numerical models and the fact remains that A' does not represent conductivity. Hence Klein's equation is more commonly used.

3. Maximum Thermal Voltage of a Dielectric Thick Slab – Steady State

The geometry of a general dielectric thick slab is shown in the Fig. 1. In a plane-parallel geometry whose boundary planes are perfectly conducting, the heat source is only due to the leakage current flowing through the insulation. In other words, the heat is uniformly distributed along x-y plane. The voltages are also uniformly distributed along x-y plane. Hence this simplifies to one-dimensional problem.

The backbone of any field problem is continuity equation. Under steady state, the net charge accumulation in an infinitesimal volume is zero, which yields the current continuity equation.

$$\nabla.\boldsymbol{J} = 0 \Rightarrow \boldsymbol{J} = constant \quad (5)$$

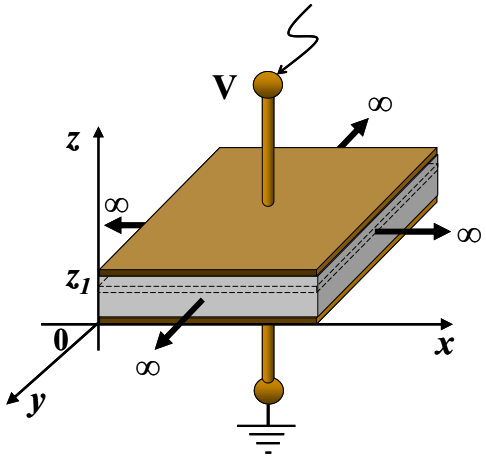

Fig. 1. Infinite dielectric thick slab

In one dimension, it reduces to,

$$J = \sigma\frac{d\Phi}{dz} \quad (6)$$

Similarly, there is no net heat accumulation inside the material under steady state, which gives thermal continuity equation.

$$(Heat\ flow) + (Heat\ generated\ by\ source) = 0 \quad (7)$$

$$-\nabla.\boldsymbol{q} + (\boldsymbol{J}.\boldsymbol{E}) = 0 \Rightarrow k_i\nabla^2 T + (\boldsymbol{J}.\boldsymbol{E}) = 0 \quad (8)$$

In one dimension, it reduces to,

$$k_i\frac{\partial^2 T}{\partial z^2} + J\frac{d\Phi}{dz} = 0 \quad (9)$$

Here J is the current density, Q heat flow and Φ potential distribution. Equations (6) and (9) are solved simultaneously with their corresponding boundary conditions to obtain field (E) and temperature (T) distributions.

Now the thick slab dielectric can have three different types of boundary conditions.

- Constant temperature (Dirichlet) boundaries
- Thermally sealed (one-end) boundary.
- External heat injection.

The first two conditions are already discussed in [9, 10]

by Whitehead and O'Dwyer, and will be briefly touched upon. The third condition however is more practically relevant, since heat is injected into dielectric due to ohmic losses from current carrying conductors.

A. Constant temperature boundaries (Whitehead and O'Dwyer)

As shown in the Fig. 2, in constant boundary temperature conditions, heat flows in both directions, normal to the notional mid-plane. Hence it is reasonable to assume that the hotspot occurs at midpoint.

The potential at the mid plane is $V/2$. This leads to a boundary condition.

$$k_i \frac{dT(z)}{dz}|_{z=0^+} = k_i \frac{dT(z)}{dz}|_{z=z_1^-} = \frac{1}{2}VJ \quad (10)$$

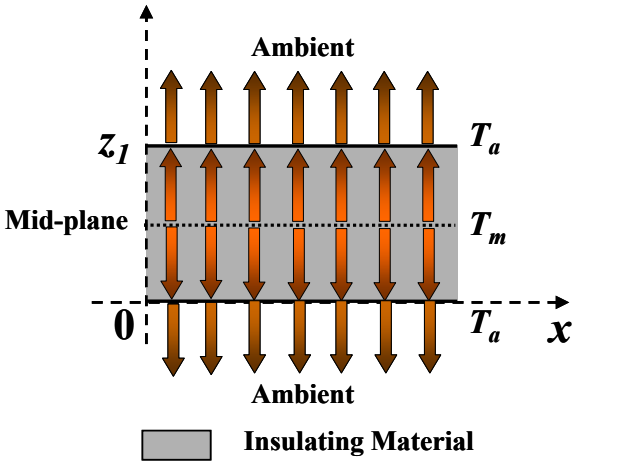

Fig. 2. Heat flow pattern when both boundaries are exposed.

Solving equations (6), (9) and (10) and integrating until critical temperature(T_c) yields maximum thermal voltage(V_{m1}).

$$V_{m1}^2 = \int_{T_a}^{T_c} \frac{8k_i}{\sigma} dT \quad (11)$$

B. Thermally sealed boundary (Whitehead and O'Dwyer)

As shown in the Fig. 3, if one end of dielectric is thermally sealed, the heat flow is restricted to single direction. The hotspot will be at sealed boundary.

Hence the boundary conditions change to:

$$k_i \frac{dT(z)}{dz}|_{z=0^+} = VJ \quad (12)$$

And

$$k_i \frac{dT(z)}{dz}|_{z=z_1^-} = 0 \quad (13)$$

Again solving equations (6), (9), (12) and (13), and integrating until critical temperature(T_c) in the similar manner, yields maximum thermal voltage(V_{m2}).

$$V_{m2}^2 = \int_{T_a}^{T_c} \frac{2k_i}{\sigma} dT \quad (14)$$

We can immediately observe that the maximum thermal voltage is exactly halved when compared to previous case, provided all other parameters remain the same.

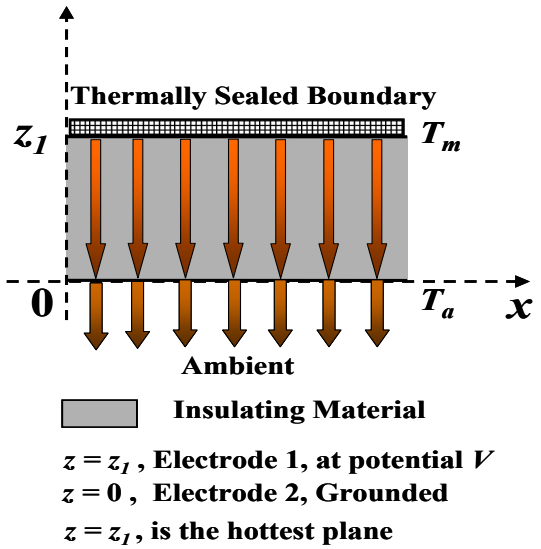

Fig. 3. Heat flow pattern when one boundary is sealed.

C. External Heat Injection (Author's Emendation)

Practical cables rarely follow Dirichlet temperatures. Heat is always injected externally into the insulation due to ohmic losses of the conductor. Such case is diametrically different from previous two.

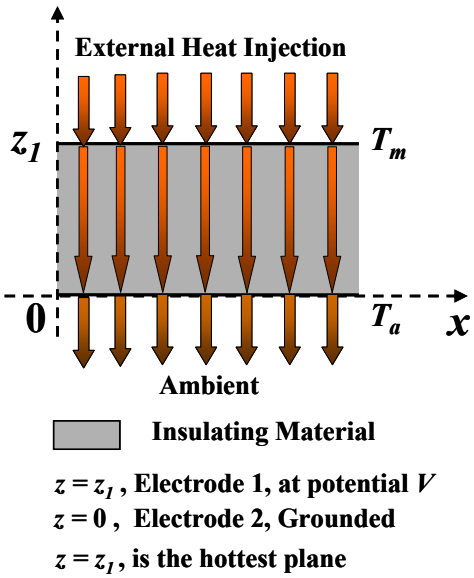

Fig. 4. Heat flow pattern with external heat injection.

The temperature is maximum at the point of injection. If Q is the heat injected per unit surface area, then the boundary conditions would be:

$$k_i \frac{dT(z)}{dz}|_{z=z_1^-} = Q \quad (15)$$

and

$$k_i \frac{dT(z)}{dz}|_{z=0^+} = Q + VJ \tag{16}$$

Proceeding as in previous sections, and integrating until critical temperature (T_c) yields maximum thermal voltage (V_{m3}), which is more generalized expression, that also includes boundary heat injection. This will be discussed in further detail in subsequent sections.

$$V_{m3}^2 = \int_{T_a}^{T_c} \frac{2k_i}{\sigma} dT - 2Q \int_0^{z_1} \frac{1}{\sigma} dz \tag{17}$$

4. Electric Field and Maximum Thermal Voltage of a DC Cable – Steady State

A power cable conforms to the cylindrical geometry as shown in Fig. 5. Unlike thick slab case, the conductor is always at the higher potential than sheath, unless otherwise mentioned. Hence, the heat flow pattern is always from conductor to sheath

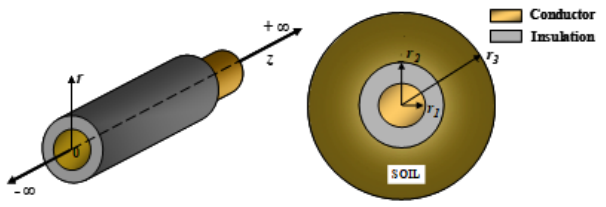

Fig. 5. 3D view and cross section of cable.

If I_L is the load current, I is the leakage current per unit length and R_c is the conductor resistance per unit length, then the thermal boundary conditions are obtained by invoking Fourier laws at boundaries.

$$2\pi r_1 k_i \frac{dT(r)}{dr}|_{r=r_1^+} = -I_L^2 R_C \tag{18}$$

And

$$2\pi r_2 k_i \frac{dT(r)}{dr}|_{r=r_2^-} = -I_L^2 R_C - VI \tag{19}$$

And of course, the Dirichlet boundary condition at the soil.

$$T(r_3) = T_a \tag{20}$$

The thermal continuity equation for cable is obtained in cylindrical coordinates as

$$\frac{1}{r}\frac{d}{dr}\left(rk_i \frac{dT(r)}{dr}\right) + \sigma\left(\frac{d\Phi(r)}{dr}\right)^2 = 0 \tag{21}$$

And similarly, the current continuity equation becomes

$$I = 2\pi r\sigma \frac{d\Phi(r)}{dr} \tag{22}$$

Solving as in previous sections until critical temperature(T_c) yields maximum thermal voltage(V_{mc})

$$V_{mc}^2 = \int_{T_a}^{T_c} \frac{2k_i}{\sigma} dT - \frac{I_L^2 R_C}{\pi} \int_{r_1}^{r_2} \frac{1}{r\sigma} dr \tag{23}$$

$$\Rightarrow V_{mc}^2 = V_{m2}^2 - \frac{I_L^2 R_C}{\pi} \int_{r_1}^{r_2} \frac{1}{r\sigma} dr \tag{24}$$

We can observe the similarity between the expressions of maximum thermal voltage for thick slab with external heat and cable with load current. For a given voltage, instability or failure would occur when load current is increased beyond certain limits. Hence thermal instability in DC cables is decided by both voltages and load currents.

If R_i is the bulk resistance per unit length of the cable, then equation (24) can be compacted to

$$V_{mc}^2 = V_{m2}^2 - 2I_L^2 R_C R_{ic} \tag{25}$$

Here R_{ic} is the bulk resistance when temperature reaches its critical value

$$R_{ic} = \int_{r_1}^{r_2} \frac{dr}{2\pi r\sigma} \tag{26}$$

Equation (25) can be rewritten as

$$V_{mc} \approx V_{m2}\left(1 - \frac{I_L^2 R_C R_{ic}}{V_{m2}^2}\right) \tag{27}$$

Or, the estimated reduction in maximum thermal voltage due to load effect is given by:

$$\Delta V_{mc} = \frac{I_L^2 R_C R_{ic}}{V_{m2}^2} \tag{28}$$

The computation of maximum thermal voltage becomes complex when we consider the non-linearity of conductivity. Eoll [18] has approximated the stress dependent portion of conductivity equation to obtain the expression of electric field distribution for an oil impregnated paper cable, both with and without insulation power losses.

A. Eoll's method:

Eoll has considered a slightly different model of resistivity from Klein as shown below.

$$\rho = \rho_0 e^{-aT} e^{-kE} \tag{29}$$

Where, a and k are empirically determined constants. Also assume that

$$e^{-kE(r)} \approx \left(\frac{E(r)}{E_0}\right)^{-c} \tag{30}$$

Where $E_0$is defined by

$$E_0 = \frac{\Phi}{e(r_2 - r_1)} \tag{31}$$

Here c is chosen so that the approximation is as accurate as possible when E_0 takes such a value. One estimate for c is given by

$$c = \frac{k\Phi}{r_2 - r_1} \tag{31}$$

Without considering power losses in insulation, the electric stress is given by

$$E(r) = \left[\frac{I\rho_0}{2\pi r_2} e^{-aT(r_2)}\right]\left(\frac{r}{r_2}\right)^{b-1} e^{-kE(r)} \tag{33}$$

And the breakdown voltage is simply obtained by

$$V_{mc} = \int_{r_1}^{r_2} E(r)dr \tag{34}$$

Where

$$b = \frac{aW_c}{2\pi k_i} \tag{35}$$

And W_c are conductor losses per unit length. Eoll's results will be discussed in more detail in subsequent sections.

B. Author's method:

Unlike Eoll's method, the author uses mean value theorem to obtain the closed form expression for maximum thermal voltage with non-linear conductivity.

Let the conductivity be defined as product of arbitrary functions of field and temperature.

$$\sigma = \sigma_0 f(T) g(E) \tag{36}$$

Now from equation (14) and (36) we have,

$$V_{m2}^2 = \int_{T_a}^{T_c} \frac{2k_i}{\sigma_0 f(T) g(E)} dT \tag{37}$$

If d is the insulation thickness and $E_0 = \frac{V_{m2}}{d}$, then from mean value theorem, we obtain:

$$V_{m2}^2 = \frac{1}{g(\eta E_0)} \int_{T_a}^{T_c} \frac{2k_i}{\sigma_0 f(T)} dT \tag{38}$$

where $\eta E_0 = E(r_m)$ for some known values of η and r_m in $r_1 \le r_m \le r_2$

$$V_{m2}^2\, g(\eta \frac{V_{m2}}{d}) = \frac{2k_i}{\sigma_0} \int_{T_a}^{T_c} \frac{1}{f(T)} dT \tag{39}$$

η can be any random number depending on the linearity of field distribution, $0 < \eta < 2$. $\eta = 1$ is often the most reasonable choice.

Using similar approach, the critical insulation resistance is found out to be:

$$R_{ic} = \frac{1}{2\pi\sigma_0 g(\eta \frac{V_{m2}}{d})} \int_{r_1}^{r_2} \frac{dr}{r f(T)} \tag{40}$$

Now, a logarithmic temperature distribution is essential for this approach.

$$T(r) = T_a + (T_c - T_a) \frac{ln\left(\frac{r}{r_2}\right)}{ln\left(\frac{r_1}{r_2}\right)} \tag{41}$$

Substituting equation (41) in (40) will yield closed form solution for critical insulation resistance. Since the conductivity has positive temperature coefficients, it accounts for positive feedback of thermal runaway.

C. Temperature distribution of DC cable

Rewriting equation (22) in terms of leakage current and separating $E(r)$ and $T(r)$, we get:

$$\ln\big(E(r)\big) + aE(r) = ln\left(\frac{I}{2\pi r A}\right) + \frac{b}{T(r)} \tag{42}$$

Now, expanding the above equation into Taylor's series onto some known values E_0 and T_0 for up to two terms, and simplifying, we get:

$$E(r) = b_1 + b_2 \ln(r) + b_3 T(r) \tag{43}$$

Where

$$b_1 = -b_2 \left(ln\left(\frac{I}{2\pi A E_0}\right) + 1 + \frac{2b}{T_0}\right) \tag{44}$$

$$b_2 = \frac{-E_0}{aE_0 + 1} \tag{45}$$

$$b_3 = b_2 \frac{b}{T_0^2} \tag{46}$$

Thus the heat continuity equation (21) can be modified and rearranged by substituting equation (43)

$$\frac{d^2T(r)}{dr^2} + \frac{1}{r}\frac{dT(r)}{dr} - \frac{\beta}{r} T(r) = \frac{1}{r}(\gamma \ln(r) - \alpha) \tag{47}$$

Where $\alpha = k_1 b_1, \beta = -k_1 b_3, \gamma = -k_1 b_2$ and $k_1 = \frac{I}{2\pi k_i}$

This is an inhomogeneous modified Bessel's equation whose solution is given by

$$T(r) = a_1 I_0\big(2\sqrt{\beta r}\big) + a_2 K_0\big(2\sqrt{\beta r}\big) + \frac{\alpha}{\beta} - \frac{\gamma}{\beta}\ln(r) \tag{48}$$

Where a_1 and a_2 are arbitrary constants determined by boundary conditions, and I_0 and K_0 are the modified Bessel functions of zero order.

D. Electric field distribution of a DC cable

Computing electric field distribution is just straightforward back substitution of $T(r)$ in equation (42), which yields:

$$E(r) = \frac{-c_2}{2c_1} \pm \sqrt{\frac{c_2^2}{4c_1^2} - \frac{1}{c_1}\left(\ln\left(\frac{I}{2\pi r A E_0}\right) + \frac{b}{T(r)} + \frac{3}{2}\right)} \tag{49}$$

where $c_1 = \frac{1}{2E_0^2}$ and $c_2 = \frac{-2 - aE_0}{E_0}$.

E. Mapping electric field and temperature distributions

The details of the cable used by the author are listed below:

- r_1 = 22.5 mm, r_2 = 44.2 mm, r_3 = 1m;

- R_c = 17.38 x 10^{-6} Ω / m;
- k_i = 0.34 W/mK, k_s = 1 W/mK;
- A = 2.2896 x 10^{-6} (Ω. m)$^{-1}$;
- a = 0.142 x 10^{-6} (V/m)$^{-1}$, b =7600 (^{0}K);
- ϕ = 0.6549 e v.
- B = 1.9112 x 10^{-7} (V/m)$^{-1}$;
- $A^{'}$ = 3.41118862 x 10^2 V / (Ω m^2);

Using equations (37), (48) and (49), the electric field and temperature distributions are obtained at different voltages and load currents. First, they are computed at 600 kV for different load currents are plotted in Fig. 6.

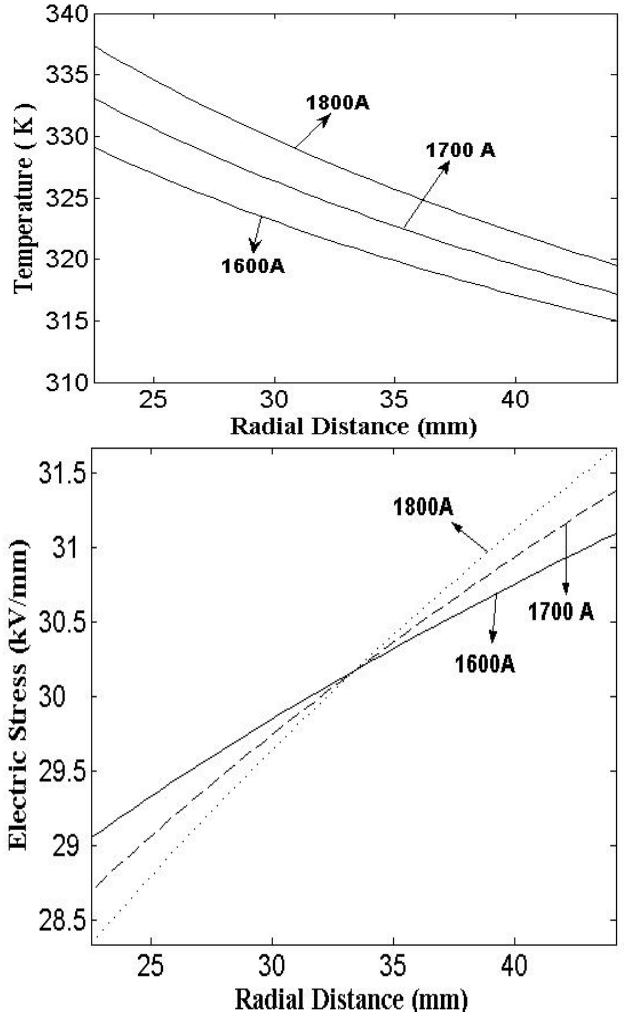

Fig. 6. Temperature and Electric Stress distributions at different load currents.

We can see that $E(r)$ is a strong function of load current unlike AC case and clearly observe the field inversion effects. Now, the field and temperature distributions are plotted with increasing voltages until critical limits in Fig. 7.

The stress distribution is more or less linear until the critical point, where it begins to fold into two solutions. The upper fold corresponds to higher leakage current regime and is unstable. The lower fold yields stable solution, however the temperature beings to increase dramatically after the critical point. This criticality is termed as maximum thermal voltage. This phenomenon is better illustrated in Fig. 8, where peak temperature and field is plotted with increasing voltages, load currents and sheath temperatures.

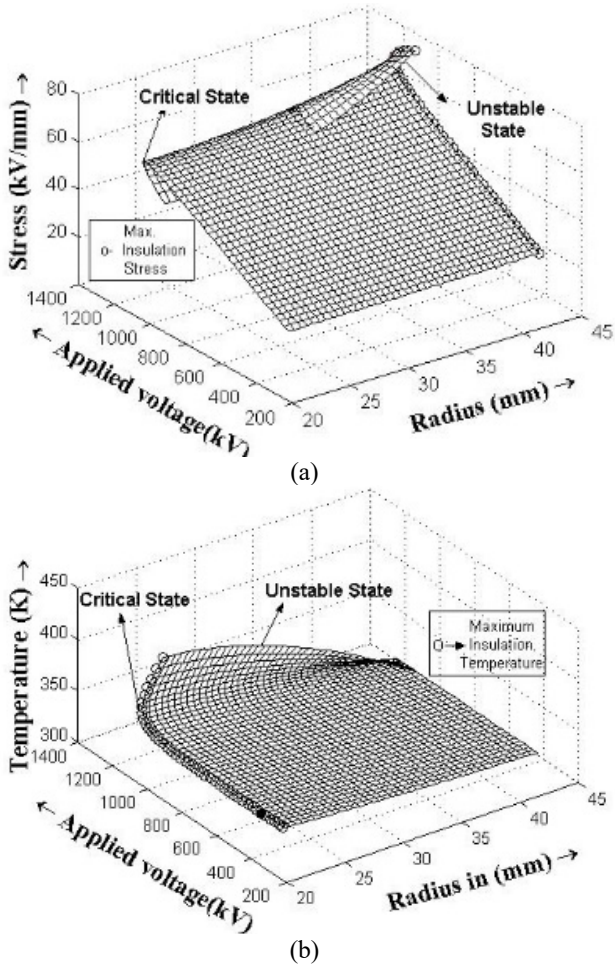

Fig. 7. (a) Temperature and (b) Electric Stress distributions with applied voltage until critical limits.

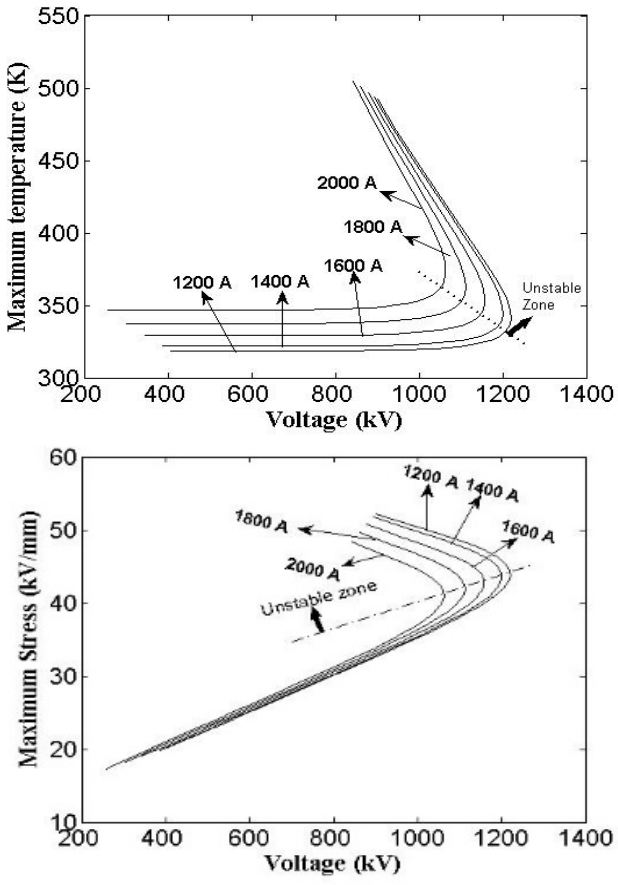

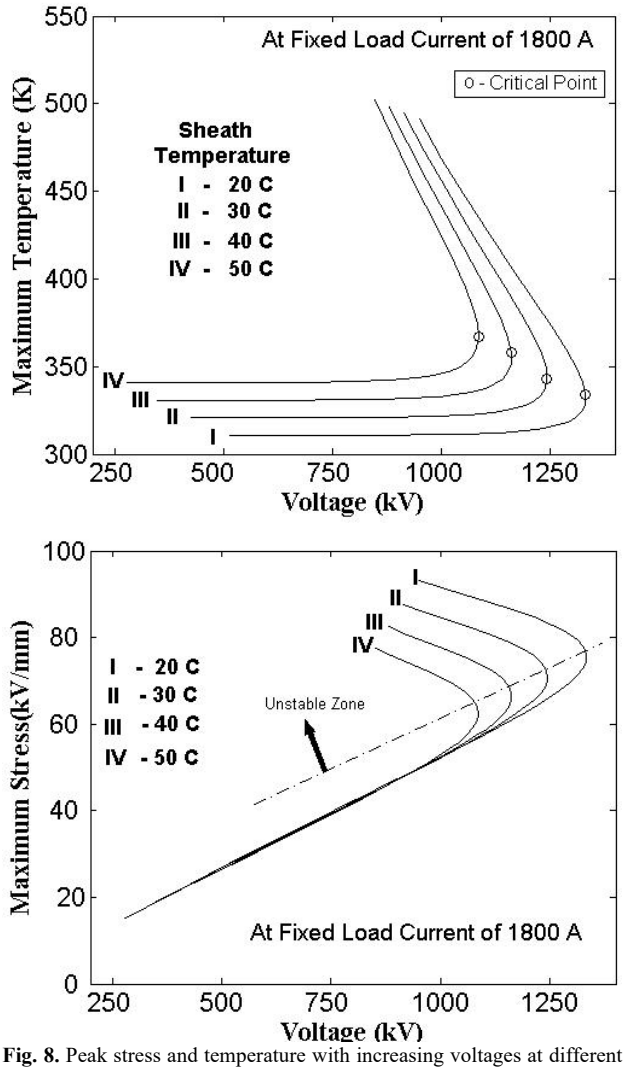

Fig. 8. Peak stress and temperature with increasing voltages at different load currents and sheath temperatures.

F. Intrinsic thermal instability of DC cables

External thermal resistance also plays an important role in deciding the thermal instability of the insulation. Even when the ambient environment (soil) is assumed to be of zero thermal resistance, the unstable conditions still persist, save for the difference in their magnitudes. This type of thermal instability in cables was first addressed by Eoll [21, 22].

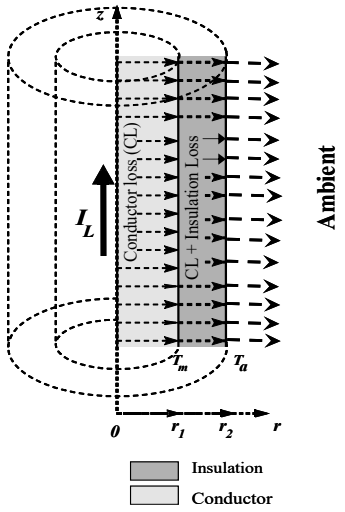

Fig. 9. Heat flow patterns in DC cable.

Referring to Fig. 9, the thermal boundary conditions are quite similar to that of section IV.

$$2\pi r_1 k_i \frac{dT(r)}{dr}|_{r=r_1^+} = -I_L^2 R_C \tag{50}$$

However, since the external thermal resistance is zero, temperature at $r = r_2$ is ambient temperature.

$$T(r_2) = T_a \tag{51}$$

Now the dc conductivity at any position r can be estimated using already established field and temperature distributions (equations (48) and (49)). The steady state voltage across the insulation can now be written in terms of leakage current and bulk resistance as

$$V = R_i I \tag{52}$$

Now, from Fig. 10, we can observe that the bulk insulation resistance monotonically decreases with leakage current, until a certain point, after which, the decrement of bulk resistance is much more rapid than increment of leakage current.

At the point of maxima, the product of bulk resistance and leakage current is maximum, which corresponds to intrinsic maximum thermal voltage (IMTV). Application of voltages higher than this result in imminent thermal instability.

Intrinsic instability is a direct consequence of stress and temperature dependence of conductivity, in other words, for a given sheath temperature, IMTV is purely material dependent.

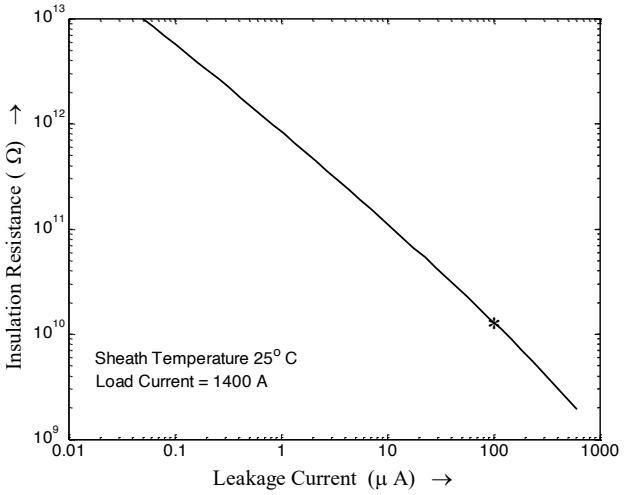

Fig. 10. Dependence of bulk insulation resistance on leakage current.

It is the ultimate upper limit of a cable. Interactive thermal instability on the other hand occurs due to the failure of thermal equilibrium with surroundings (non-zero external thermal resistance), in addition to the nonlinear conductivity, hence Interactive maximum thermal voltage is lower.

G. Dependence of thermal breakdown strength on insulation thickness

It is generally believed that the breakdown strength of insulation has only marginal dependence on insulation thickness [9]. However, it is only true for plane-parallel geometry case where conductivity is only a function of temperature. In dc cables (cylindrical geometry) where

conductivity has radial dependence with electric field and temperature, breakdown strength does depend on insulation thickness. This is further enhanced due to field inversion occurring in dc cables.

The conductor radius (r_1) and sheath temperature $T(r_2)$ are kept constant at 22.5 mm and 25^{0}C respectively, while the outer radius (r_2) is varied corresponding to different insulation thicknesses.

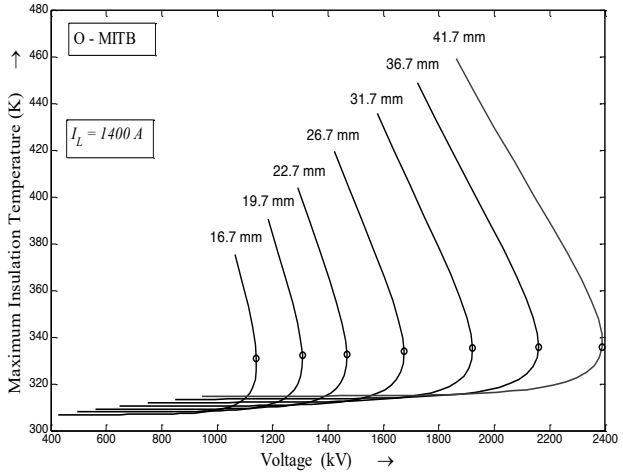

Fig. 11. Maximum insulation temperature with increasing thickness.

Fig. 11 shows the variation of maximum insulation temperature with voltage at different thicknesses. With increasing thickness, the maximum insulation temperature curves seem to have shifted up. This is due to the fact that thermal resistance of insulation increases with thickness.

The maximum insulation stress curves are plotted with voltage at different thicknesses in Fig. 12, and the critical maximum and average stresses (or breakdown stress) are plotted with thickness in Fig. 13. We can observe how both the maximum and average breakdown stress decrease with insulation thickness, despite the increase in ITMV.

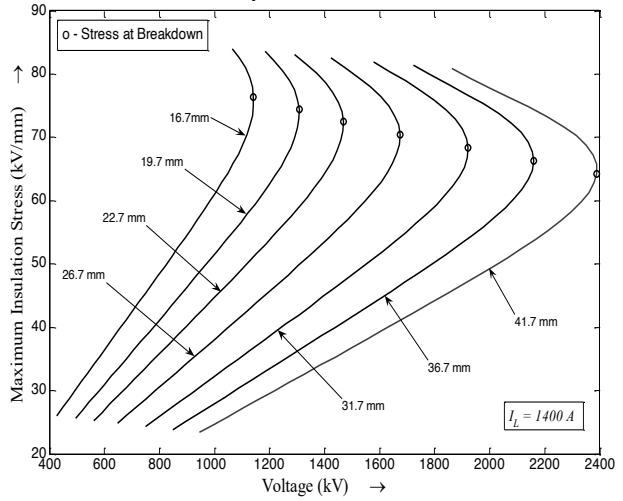

Fig. 12. Maximum insulation stress with increasing thickness.

H. Comparison of Author's and Eoll's methods:

The variation of MTV with load current at increasing sheath temperatures and MTV with sheath temperature at constant load current is plotted in Fig. 14.

The authors results are found to be in close conformity with Eoll's results on oil impregnated paper cables. Eoll has worked on two types of cables shown in table I, with a slightly different conductivity model (equation (29)).

Eoll's and authors results for cable 1 data is shown in Fig. 15. Eoll has assumed an intrinsic breakdown strength of 1.2 x 10^8 V/m, which is the reason for steep deviation in Eoll's results at lesser sheath temperatures. The Authors results more or less match with Eoll's barring that constraint.

The authors results were also compared with Eoll's results for cable 2 data, which are again observed to be in close conformity with each other.

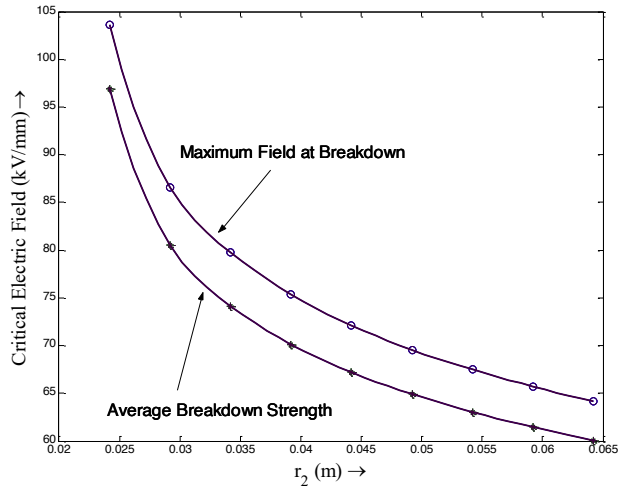

Fig. 13. Maximum and average stresses with increasing thickness.

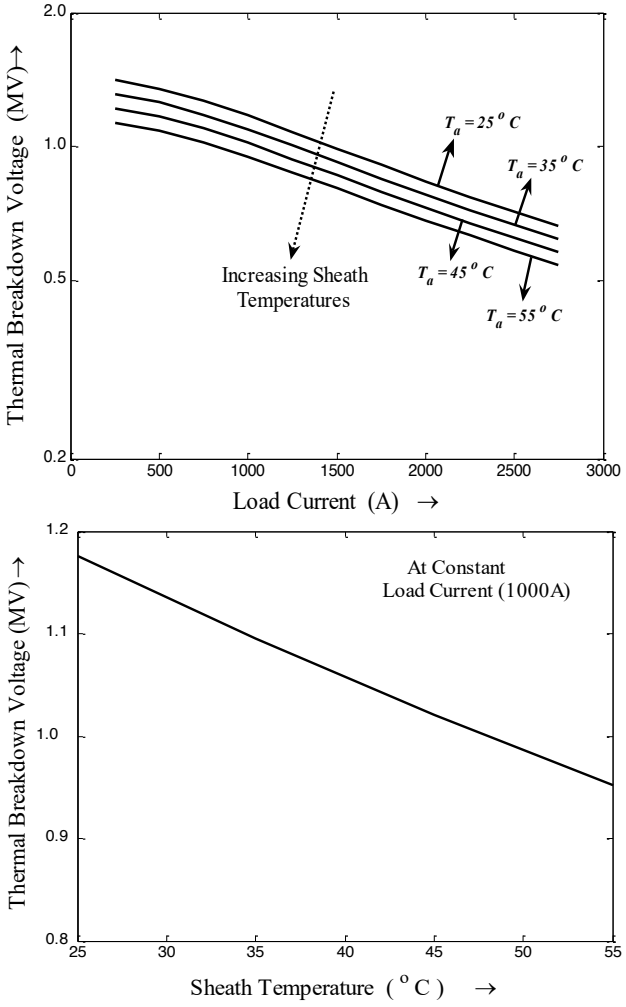

Fig. 14. Variation of MTV with load current and sheath temperatures.

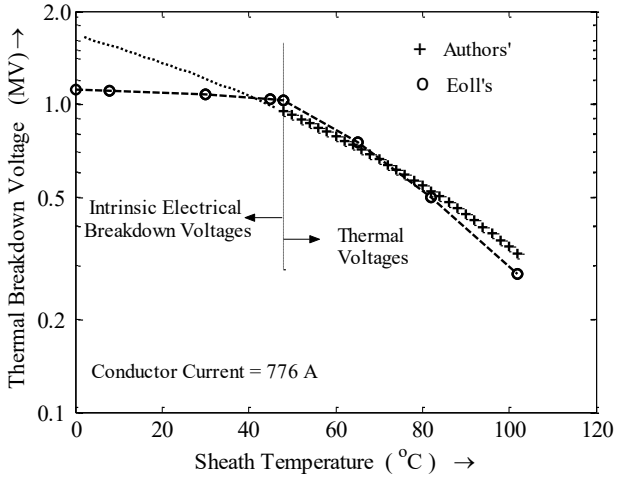

Fig. 15. Comparison of Eoll's and Author's results for cable 1.

5. V. Transient Behavior of a DC Cable

Obtaining a closed form analytical solution of electric field and temperature for a DC cable in transient conditions is wrought with utmost mathematical complexity. Even a numerical solution is challenging enough. Hence all the FEM/circuit models hitherto [29-35] were approximations, be it neglecting leakage current losses, or not considering non-linear conductivity, or lumping thermal capacitances and so on and so forth. In this section, a proper distributed circuit model for both thermal and electrical phenomena of a DC cable considering non-linear conductivity and thermal-electrical interdependence is discussed.

A. Electro-thermal circuit model of a DC cable

Since thermal quantities such as heat flow, temperature and thermal conductivity are analogous to their respective electrical quantities such as current flow, voltage and electrical conductivity, the thermal behavior of cable can be modelled with their equivalent distributed electrical parameters. Fig. shows the DC cable with all its layers and Fig. 16, shows how they can be modelled by dividing into several concentric cylindrical strips/elements.

All the quantities are in the form M_γ^δ, where

M – small letter denotes thermal quantity, block letter denoted electrical quantity
γ – denotes the node/section number
δ – denotes the type of layer ('c'- conductor, 'cs'- conductor screen, 'i' - insulation, 'is'- insulation screen, 'wr'- water resistant layer, 'sh'- sheath, 'os'- outer serving and 'su'- surrounding medium)

The thermal resistance per unit length between nodes γ and $\gamma+1$ is given by

$$r_\gamma^\delta = \frac{log\left(\frac{d_{\gamma+1}}{d_\gamma}\right)}{2\pi k_\gamma^\delta} \tag{53}$$

The variation of the thermal conductivity$\left(k_\gamma^\delta\right)$ with temperature$\left(v_\gamma^\delta\right)$ is taken into account by

$$k_\gamma^\delta = k^\delta + \alpha^\delta\left(v_\gamma^\delta - 293\right) \tag{54}$$

The thermal capacitance per unit length is given by

$$c_\gamma^\delta = \pi\left[\left(d_{\gamma+1}\right)^2 - \left(d_\gamma\right)^2\right]\rho^\delta s^\delta \tag{55}$$

The heat source in conductor and insulation are represented as current sources in thermal circuit, which are in turn just I^2R losses in electric circuit.

$$i_\gamma^c = \left(I_\gamma^c\right)^2 R_\gamma^c \tag{56}$$

$$i_\gamma^i = \left(I_\gamma^i\right)^2 R_\gamma^i \tag{57}$$

These ultimately comprise the thermal circuit of a DC cable as shown in Fig. 18. The electrical circuit on the other hand is straightforward. The resistance per unit length of conductor is modeled around the standard resistivity ρ_0 at standard temperatures (293 K).

$$R_\gamma^c = \frac{\rho_0\left(1+\alpha\left(\frac{v_\gamma + v_{\gamma+1}}{2} - 293\right)\right)}{\pi\left(\left(d_{\gamma+1}\right)^2 - \left(d_\gamma\right)^2\right)} \tag{58}$$

The resistance per unit length of insulation can be written as:

$$R_\gamma^i = \frac{\log\left(\frac{d_{\gamma+1}}{d_\gamma}\right)}{2\pi\sigma} \tag{59}$$

Now substituting equation () we get

$$R_\gamma^i = \frac{\log\left(\frac{d_{\gamma+1}}{d_\gamma}\right)e^{\left(\frac{b}{v_\gamma} - a|E_\gamma|\right)}}{2\pi A} \tag{60}$$

The electric field in the strip can be estimated as

$$E_\gamma \approx \frac{V_\gamma - V_{\gamma+1}}{\left(d_{\gamma+1} - d_\gamma\right)} \tag{61}$$

The electrical capacitance of insulation is modeled with constant permittivity

$$C_\gamma^i = \frac{2\pi\varepsilon_0\varepsilon_r}{\log\left(\frac{d_{\gamma+1}}{d_\gamma}\right)} \tag{62}$$

The electrical circuit of conductor and insulation is ultimately shown in the Fig. 17.

B. Cables used in the simulation

A 400 MW, bipolar, $\pm 200\ kV$, 500 mm^2, HVDC cable is used for simulation. Its physical parameters are listed in table III.

C. Electric field and Temperature under step voltage

The electric field and temperature distribution for cable is shown in Figs. 19 and 20, respectively when the cable is switched on at full load.

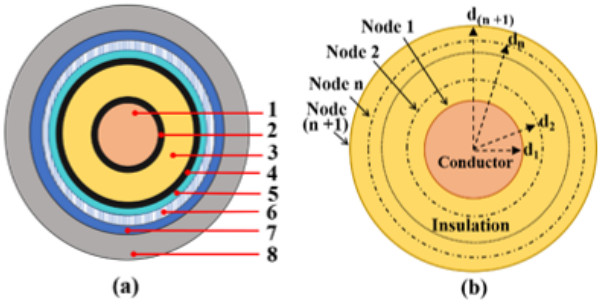

Fig. 16. (a) Sectional view of buried HVDC cable (C1) used in simulation (1-conductor (Cu-12.6 mm), 2-conductor screen (2 mm), 3-insulation (XLPE-12 mm), 4-insulation screen (1.5 mm), 5-water resistant layer (5.7mm), 6-aluminium sheath (2.3 mm) 7- PE outer serving (5 mm) and 8-soil (1 m). (b) Depiction of concentric cylinders of insulation with increasing radii from d_1 to d_{n+1} and respective node 1 to node n+1.

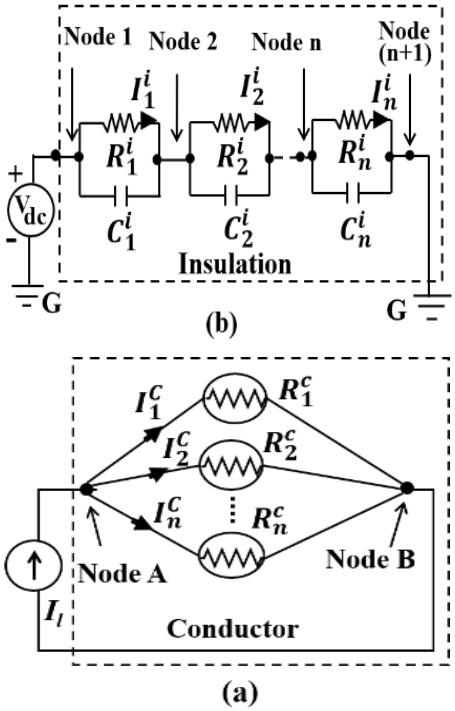

Fig. 17. Electrical circuit of (a) Conductor, (b) Insulation.

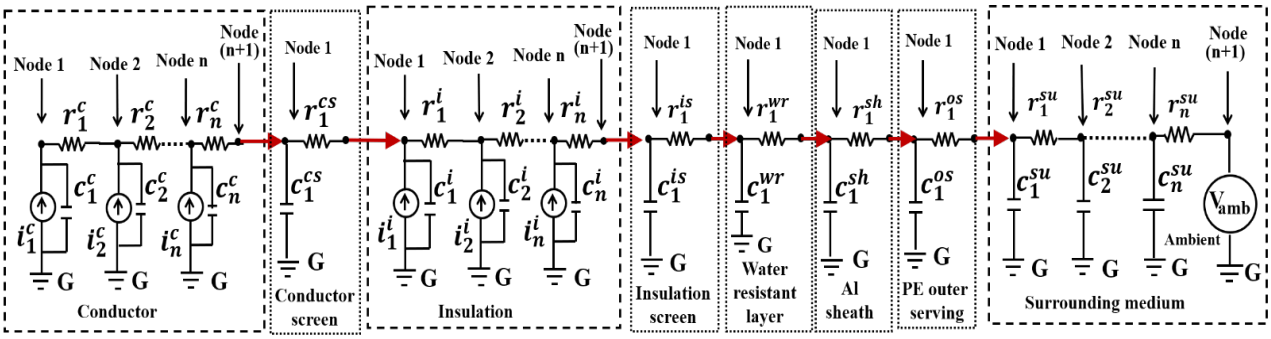

Fig. 18. Thermal circuit of a cable with all layers and surrounding medium.

Table I. Parameters of experimental cables [12]

Parameter	Cable 1	Cable 2
r_1(m)	0.0134	0.004
r_2(m)	0.0231	0.010
σ_0(S/m)	0.5 X 10^{-15}	0.5 X 10^{-15}
a (^{o}C)$^{-1}$	0.088	0.1
W_C (W/m)	17.9	0
I_L (A)	776	0
k (W m^{-1} (^{o}C)$^{-1}$)	0.167	0.167

Table II. Comparison of Eoll's and Author's results for Cable 2.

Sheath Temperature (^{0}C)	Breakdown Voltage (kV)	
	Eoll's [12] (experimental)	Author's (computed)
63	430	420.232
73	320	349.853
83	250	284.609
100	140	187.940

Table III. Physical parameters of power cable.

Quantity	Value	Quantity	Value
k^c	413 $(W/(m.K))$	k^{soil}	2.1 $(W/(m.K))$
α^c	-0.06 $(W/(m.K^2))$	s^{soil}	700 $(J/(kg.K))$
ρ^c	8960 (kg/m^3)	ρ_0	2.65 x 10^{-8} $(\Omega.m)$
s^c	390 $(J/(kg.K))$	α	0.0039 (K^{-1})
k^i	0.33 $(W/(m.K))$	k^{oil}	0.11 $(W/(m.K))$
α^i	-1.53 x 10^{-4} $\left(\frac{W}{m.K^2}\right)$	s^{oil}	1860 $(J/(kg.K))$
ρ^i	920 (kg/m^3)	ρ^{oil}	877 (kg/m^3)
s^i	2200 $(J/(kg.K))$	A	2×10^{-11} (S/m)
ε_0	8.854x 10^{-12} (F/m)	a	7×10^{-08} (m/V)
ε_r	2.25	b	3.7×10^3 K
ρ^{soil}	2270 (kg/m^3)	l	1 (m)

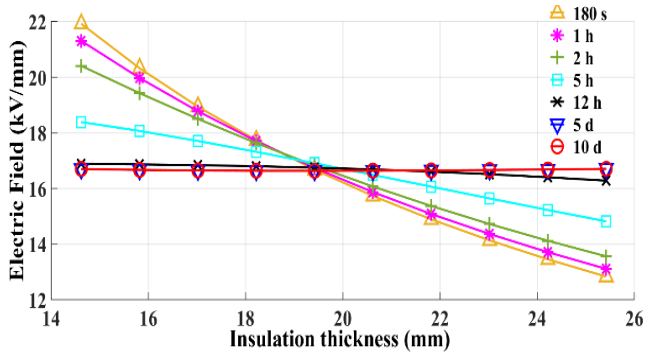

Fig. 19. Temperature distribution across cable insulation at full load for different time instants after switch on.

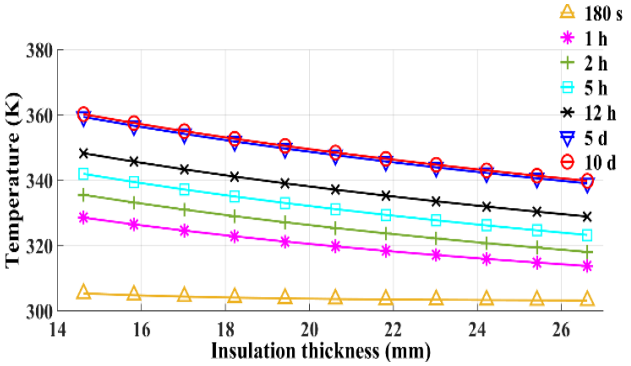

Fig. 20. Electric Field distribution across cable insulation at full load for different time instants after switch on.

It is immediately obvious that temperature takes much more time to stabilize than electric field. This happens because $\triangle T$ (which determines the electric field) stabilizes faster than T which can be seen in Figs. 21 and 22 respectively

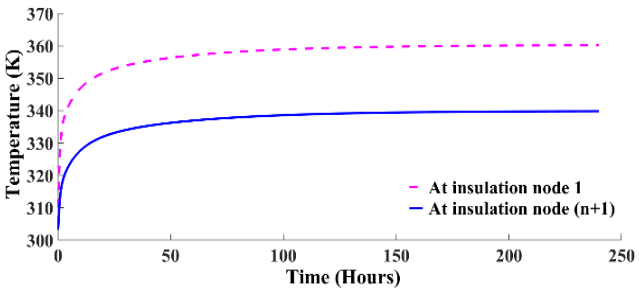

Fig. 21. Boundary temperature stabilization after switch on.

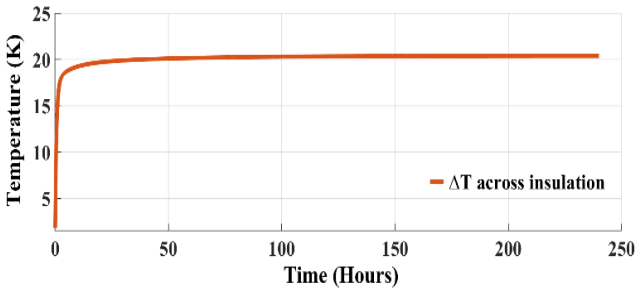

Fig. 22. $\triangle T$ stabilization after switch on.

The steady state temperature and field for different load currents is shown in Figs. 23 and 24 respectively. Stress inversion phenomena can be observed as reported in previous literature [20], though the peak field at full load is not as high as peak field at no load.

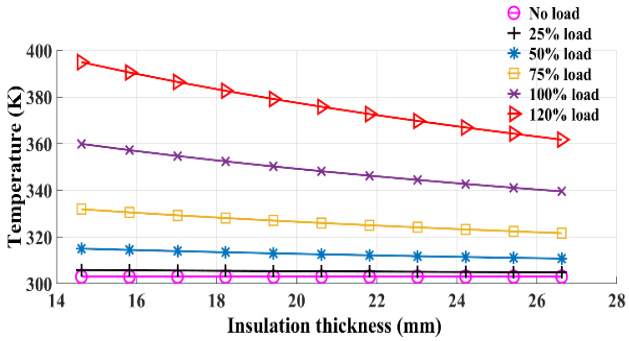

Fig. 23. Steady state temperature distributions at different load currents.

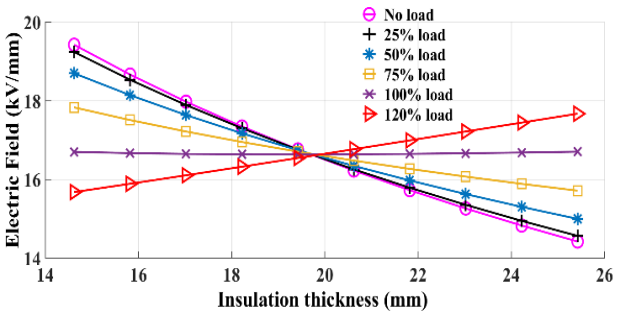

Fig. 24. Steady state field distributions at different load currents.

D. Electric field and Temperature under load cycle

A typical load cycle of heating for 240 hours (load) followed by natural cooling (no-load) for 240 hours is considered. The corresponding field and temperature distributions are shown in Figs. 25 and 26 respectively.

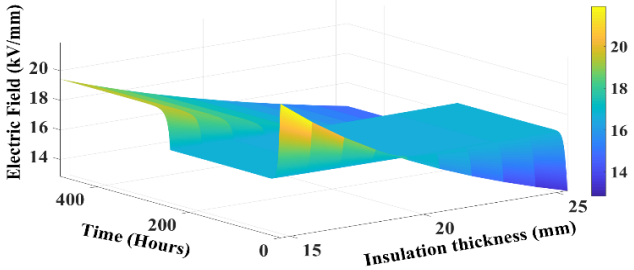

Fig. 25. Electric field distribution at load cycle.

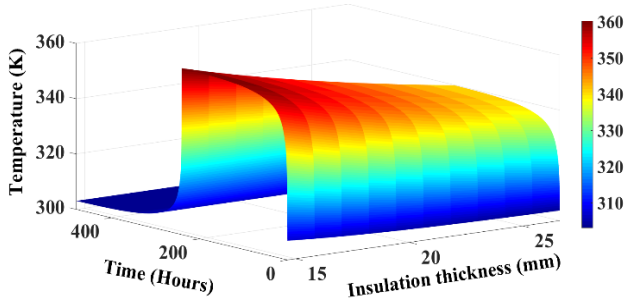

Fig. 26. Temperature distribution at load cycle.

The electric fields near conductor and sheath are also shown in Fig. 27. The peak field is high during switch on because it assumes Laplacian field distribution, but it soon changes to resistive distribution during steady state.

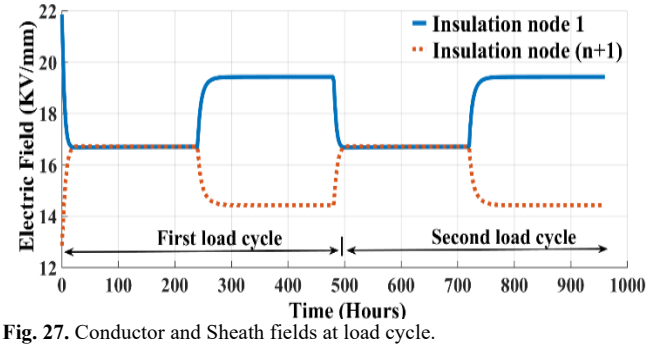

Fig. 27. Conductor and Sheath fields at load cycle.

E. Simulation of breakdown of DC cable

The cable is simulated at a step voltage equal to its MTV until breakdown. The ambient temperature is fixed at 30^0C. The dynamic field and temperature distribution during breakdown are shown in Figs. 29 and 30 respectively

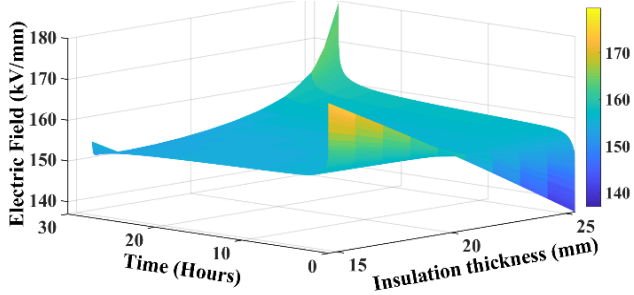

Fig. 29. Electric field distribution at breakdown.

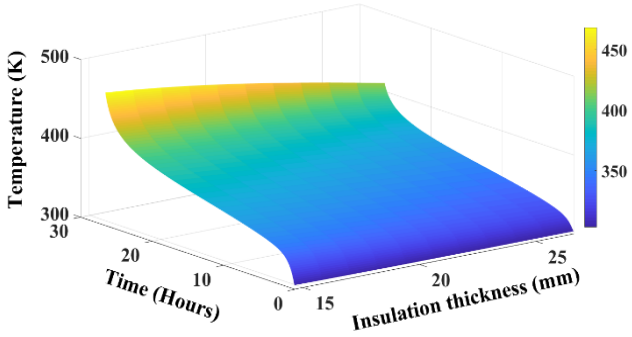

Fig. 30. Temperature distribution at breakdown.

The peak temperature and electric field in the insulation increase drastically before breakdown, indicating that even in thermal breakdown electric field increases before breakdown. The runaway phenomenon is better illustrated in Figs. 31-33 respectively, for leakage current, peak field and peak temperature.

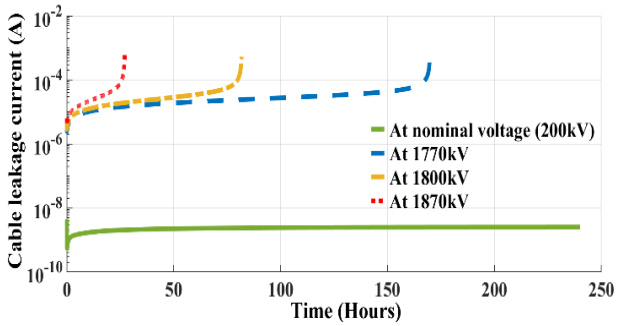

Fig. 31. Leakage current runaway at different applied voltages.

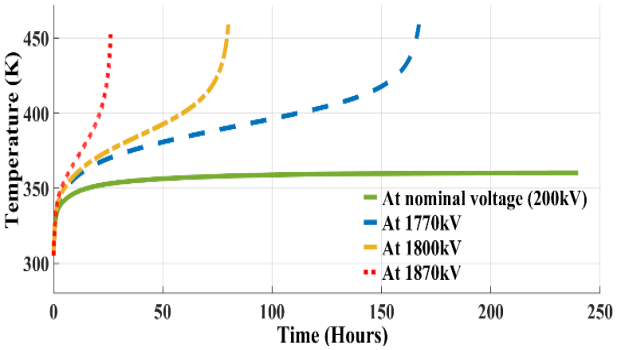

Fig. 32. Temperature runaway at different applied voltages.

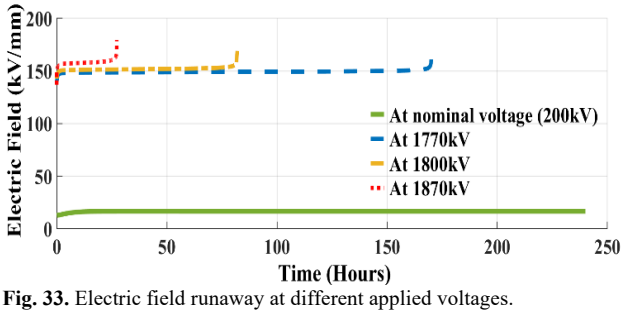

Fig. 33. Electric field runaway at different applied voltages.

The load effects on time to breakdown is illustrated in Fig. 34. This might look similar to volt-time (life) characteristics, but it is not to be confused with life characteristics, as no

ageing is involved here. These are purely the characteristics of transient thermal breakdown.

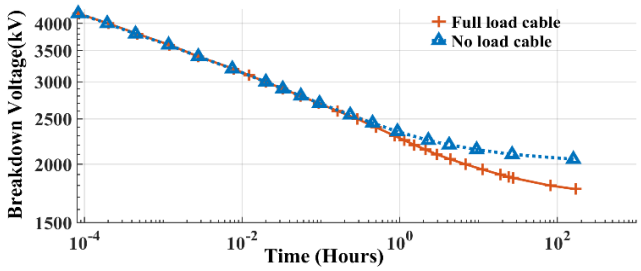

Fig. 34. Voltage vs time to breakdown characteristics for cable under no load and loaded conditions.

Time to breakdown decreases with voltage magnitude and the load effects are much severe at higher breakdown times. The effect of soil thermal resistance on breakdown is also observed, which is shown in Fig. 35, both at load and no-load conditions.

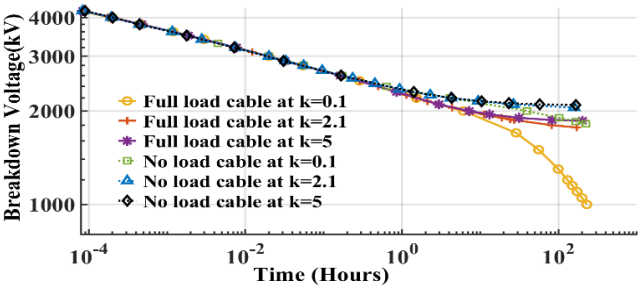

Fig. 35. Voltage vs time to breakdown characteristics at different soil thermal conductivities (external thermal resistances).

Hence the back fill of the cable assumes huge significance, as the breakdown voltages are heavily dependent on external thermal conductivities.

F. Special setup for cable breakdown and few results

The conventional cable breakdown setup involves copper strips; however, it is wrought with edge breakdown. The authors have designed a special electrode setup so that breakdown occurs at the center and the breakdown value reflects its true insulation withstand capability.

The authors have also conducted several breakdown tests on 1.1 kV XLPE cables (of 6 mm^2 conductor diameter and 0.7 mm insulation thickness) and few results at varying load currents (at constant ambient temperature of 50^{0}C) are shown in the Fig. 36.

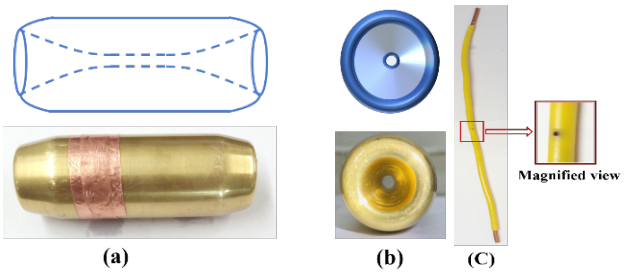

Fig. 35. Special high voltage electrode used for cable breakdown (a) top view, (b) front view. (c) Punctured XLPE cable.

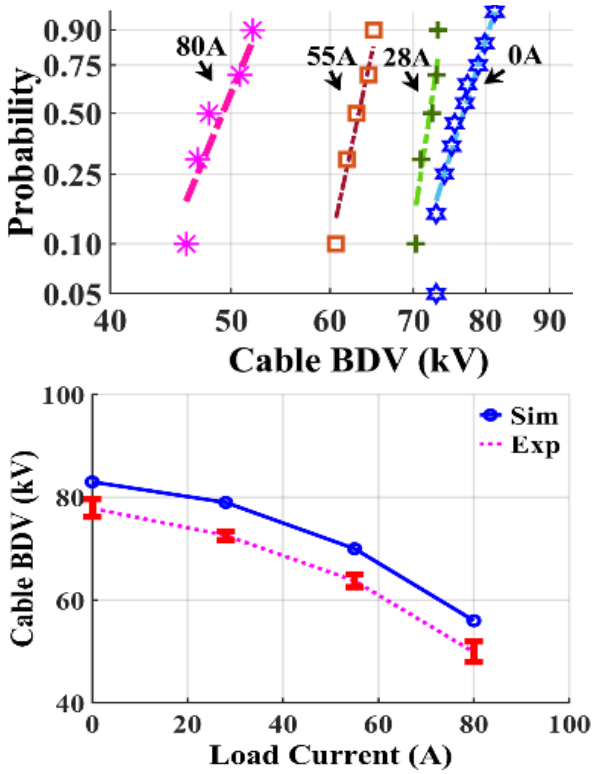

Fig. 36. Breakdown voltages and 63% breakdown values with load current.

6. Conclusions

The problem of thermal breakdown in DC cables is evergreen and relevant, especially with the increase in polymeric cable installations, be it due to the advent of renewable energy sources such as offshore energy wind turbines, or due to smart grids, and with everchanging voltage shapes due to power electronic converters.

References

[1] Semenoff and Walther, Die physikalischen grundlagen der elektrischen Festigkeitslehre, Springer, p. 126, 1928.
[2] Frohlich, Pelzer and Zienau, Phil. Mag., vol 41, p. 221, 1950
[3] Whitehead. S and Nethercot, Proceedings of Phis. Soc., vol 45, pp974, 1935.
[4] Von Hippel and Maurer. Phys. Rev., vol 59, pp 820, 1941
[5] Austen and Whitehead. S, Proc. Roy. Soc. A, vol 176, 33 1940
[6] Austen, part (i), J. I. E. E., Vol 92, pp 373, 1945
[7] Austen and Pelzer, Ibid., part I, vol 93, p 487, 1946
[8] Inge and Walther, C. R. Academy of Sciences, U. S. S. R, vol 2, pp 68, 1934
[9] Whitehead. S, Dielectric Breakdown of Solids, Oxford University Press, London, 1951.

[10] J. J. O'Dwyer, The Theory of Dielectric Breakdown of Solids, Oxford University Press, London, 1964.
[11] L. A. Dissado and J. C. Fothergill, Electrical degradation and breakdown in polymers, Peter Peregrinus, London, 1992.
[12] Blythe, A. R., Electrical Properties of Polymers, Cambridge University Press, 1986.
[13] X. Qi, Z. Zheng, and S. Boggs, "Engineering with Nonlinear Dielectrics", IEEE, DEIS Feature Article, Electrical Insulation Magazine, vol. 20, no. 6, pp. 27-34, 2004.
[14] J. Hjerrild, S. Boggs, J. T. Hollboll and M. Henricksen, "DC-field in solid dielectric cables under transient thermal conditions", IEEE, Intern. Conf. Solid Dielectrics, pp. 58-61, 2001.
[15] Klein.N, Adv. Electronics & Electron Phys., Vol. 26, ed. MARTON, L. (Academic Press, New York) 1969.
[16] U. Riechert, R. Vogelsang, and J. Kindersberger, "Temperature Effect on DC Breakdown of Polyethylene Cables", 12th International Symposium on High Voltage Engineering, ISH 2001, Bangalore, India
[17] M. Michel Fallou, "Perforration dielectrique par instabilite thermique des cables a courant continu", Revue Generale de LElectricite, pp. 693-695, Dec. 1959.
[18] C. K. Eoll, "Theory of Stress Distribution in Insulation of High Voltage DC Cables: Part I", IEEE Trans. Electr. Insul., Vol. 10, pp. 27-35, 1975.
[19] C. K. Eoll, "Theory of Stress Distribution in Insulation of High Voltage DC Cables: Part II", IEEE Transactions on Electrical Insulation, vol. Electrical Insulation-10 , no. 2, pp. 49-54, June, 1975.
[20] M. J. P. Jeroense and P. H. F. Morshuis, "Electric Fields in HV DC Paper-Insulated Cables", IEEE Tr. DEIS, Vol. 5, No. 2, April 1998.
[21] C. C. Reddy and T. S. Ramu, "On the computation of electric field and temperature distribution in HVDC cable insulation," in IEEE Transactions on Dielectrics and Electrical Insulation, vol. 13, no. 6, pp. 1236-1244, December 2006.
[22] C. C. Reddy and T. S. Ramu, "On the intrinsic thermal stability in HVDC cables," in IEEE Transactions on Dielectrics and Electrical Insulation, vol. 14, no. 6, pp. 1509-1515, December 2007.
[23] C. C. Reddy, "Theoretical Maximum Limits on Power-Handling Capacity of HVDC Cables," in IEEE Transactions on Power Delivery, vol. 24, no. 3, pp. 980-987, July 2009.
[24] B.X. Du, M. Xiao, J.W. Zhang, "Effect of thermal conductivity on tracking failure of Epoxy/BN composite under pulse strength", Dielectrics and Electrical Insulation IEEE Transactions on, vol. 20, no. 1, pp. 296-302, 2013.
[25] Jun-Wei Zha, Yun-Hui Wu, Si-Jiao Wang, Dong-Hong Wu, Hong-Da Yan, Zhi-Min Dang, "Improvement of space charge suppression of polypropylene for potential application in HVDC cables", Dielectrics and Electrical Insulation IEEE Transactions on, vol. 23, no. 4, pp. 2337-2343, 2016.
[26] Christoph Jörgens, Fotios Kasolis, Markus Clemens, "Numerical Simulations of Temperature Stability Limits in High-Voltage Direct Current Cable Insulations", Magnetics IEEE Transactions on, vol. 55, no. 6, pp. 1-4, 2019.
[27] Sarath Kumara, Yuriy V. Serdyuk, Marc Jeroense, "Calculation of Electric Fields in HVDC Cables: Comparison of Different Models", Dielectrics and Electrical Insulation IEEE Transactions on, vol. 28, no. 3, pp. 1070-1078, 2021.
[28] Purnabhishek Muppala, C. C. Reddy, "Electric Field and DC Breakdown Voltage of Multi-layer Dielectrics in Parallel-Plane Geometry", Dielectrics and Electrical Insulation IEEE Transactions on, vol. 28, no. 1, pp. 257-265, 2021.
[29] Y. Liu, S. Zhang, X. Cao, C. Zhang and W. Li, "Simulation of electric field distribution in the XLPE insulation of a 320 kV DC cable under steady and time-varying states," in IEEE Transactions on Dielectrics and Electrical Insulation, vol. 25, no. 3, pp. 954-964, June 2018.
[30] Y. O. Shaker, A. H. El-Hag, U. Patel and S. H. Jayaram, "Thermal modeling of medium voltage cable terminations under square pulses," in IEEE Transactions on Dielectrics and Electrical Insulation, vol. 21, no. 3, pp. 932-939, June 2014.
[31] N. Kovac, I. Sarajcev and D. Poljak, "Nonlinear-coupled electric-thermal modeling of underground cable systems," in IEEE Transactions on Power Delivery, vol. 21, no. 1, pp. 4-14, Jan. 2006.
[32] C. Garrido, A. F. Otero and J. Cidras, "Theoretical model to calculate steady-state and transient ampacity and temperature in buried cables," in IEEE Transactions on Power Delivery, vol. 18, no. 3, pp. 667-678, July 2003.
[33] T. L. Jones, "The calculation of cable parameters using combined thermal and electrical circuit models," in IEEE Transactions on Power Delivery, vol. 4, no. 3, pp. 1529-1540, July 1989.
[34] G. J. Anders and M. A. El-Kady, "Transient ratings of buried power cables. I. Historical perspective and mathematical model," in IEEE Transactions on Power Delivery, vol. 7, no. 4, pp. 1724-1734, Oct. 1992.
[35] X. Zhang and S. Pekarek, "A coupled thermal/electric circuit model for design of MVDC ship cables," 2017 IEEE Electric Ship Technologies Symposium (ESTS), Arlington, VA, 2017, pp. 71-78.
[36] S. Dhayalan and C. Chakradharreddy, "Simulation of Electro-thermal Runaway and Thermal Limits of a Loaded HVDC Cable," in IEEE Transactions on Power Delivery (Early Access).